Taylor & Francis
Taylor & Francis Group

Numerical Heat Transfer, Part A: Applications
An International Journal of Computation and Methodology

ISSN: 1040-7782 (Print) 1521-0634 (Online) Journal homepage: http://www.tandfonline.com/loi/unht20

Local thermal nonequilibrium conjugate natural convection heat transfer of nanofluids in a cavity partially filled with porous media using Buongiorno's model

Ali Tahmasebi, Mahboobe Mahdavi & Mohammad Ghalambaz

To cite this article: Ali Tahmasebi, Mahboobe Mahdavi & Mohammad Ghalambaz (2018) Local thermal nonequilibrium conjugate natural convection heat transfer of nanofluids in a cavity partially filled with porous media using Buongiorno's model, Numerical Heat Transfer, Part A: Applications, 73:4, 254-276, DOI: 10.1080/10407782.2017.1422632

To link to this article: https://doi.org/10.1080/10407782.2017.1422632

NUMERICAL HEAT TRANSFER, PART A
2018, VOL. 73, NO. 4, 254–276
https://doi.org/10.1080/10407782.2017.1422632

Taylor & Francis
Taylor & Francis Group

Local thermal nonequilibrium conjugate natural convection heat transfer of nanofluids in a cavity partially filled with porous media using Buongiorno's model

Ali Tahmasebi[a], Mahboobe Mahdavi[b], and Mohammad Ghalambaz[c]

[a]Department of Mechanical Engineering, Shahid Chamran University of Ahvaz, Ahvaz, Iran; [b]Department of Mechanical Engineering, Gannon University, Erie, Pennsylvania, USA; [c]Department of Mechanical Engineering, Dezful Branch, Islamic Azad University, Dezful, Iran

ABSTRACT

The natural convection heat transfer in a cavity filled with three layers of solid, porous medium, and free fluid is addressed. The porous medium and free fluid layers are filled with a nanofluid. The porous layer is modeled using the local thermal nonequilibrium (LTNE) model, considering the temperature difference between the solid porous matrix and the nanofluid phases. The nanofluid is modeled using the Buongiorno's model incorporating the thermophoresis and Brownian motion effects. The governing equations are transformed into a set of nondimensional partial differential equations, and then solved using finite element method in a nonuniform grid. The effects of various nondimensional parameters are discussed. The results showed that the Brownian motion and thermophoresis effects result in significant concentration gradients of nanoparticles in the porous and free fluid layers. The increase in Rayleigh (Ra), Darcy (Da), the thermal conductivity ratios for the solid wall and solid porous matrix, i.e., K_r and R_k, enhanced the average Nusselt number. The increase in the convection interaction heat transfer parameter between the solid porous matrix and the nanofluid in the pores (H) increases the average Nusselt number in the solid porous matrix but decreases the average Nusselt number in the nanofluid phase of the porous layer.

ARTICLE HISTORY
Received 10 August 2017
Accepted 25 December 2017

1. Introduction

The rise in energy consumption due to industrial development and population growth along with their consequence environmental issues has led to a complex global crisis in the world. One of the best possible solutions to alleviate this issue is through improving the efficiency of conventional energy generation technologies. This can be done through passive heat transfer augmentation techniques, which require no additional external power and usually can be implemented easily in current thermal systems. As one of the passive methods, porous inserts have found considerable interest in industrial applications. Using porous medium, heat transfer increases because of changing the distribution of flow field and resulting a thinner boundary layer. They also increase the effective thermal conductivity of the fluid, which leads to higher heat transfer rates. To this end, convective flows through porous media have gained a great deal of attention in recent years due to their wide range of engineering applications such as solar energy collectors, heat exchangers, fuel cell, drying technologies, etc. Natural convection in rectangular cavities fully or partially filled with porous media has been investigated by many researchers [1, 2]. In an early study, Beckerman et al. [3] investigated

CONTACT Mohammad Ghalambaz m.ghalambaz@iaud.ac.ir Department of Mechanical Engineering, Dezful Branch, Islamic Azad University, Dezful, Iran.
Color versions of one or more of the figures in the article can be found online at www.tandfonline.com/unht.

Nomenclature

Latin symbols

C	nanoparticle volume fraction
C_0	ambient nanoparticle volume fraction
d	wall thickness (m)
D	dimensionless wall thickness
Da	Darcy number
D_B	Brownian diffusion coefficient
D_T	Thermophoretic diffusion coefficient
g	gravitational acceleration vector (m s^{-2})
h_{nfs}	volumetric heat transfer coefficient between the nanofluid and solid porous matrix (W m^{-3} K^{-1})
H	interface heat transfer coefficient parameter
k	thermal conductivity (W m^{-1} K^{-1})
K	permeability of the porous medium (m^2)
K_r	nanofluid to solid porous matrix thermal conductivity ratio parameter
L	square cavity size (m)
Le	Lewis number
Nb	Brownian motion parameter
Nr	buoyancy ratio parameter
Nt	thermophoresis parameter
Nu	local Nusselt number
$\overline{\mathrm{Nu}}$	average Nusselt number
p	pressure (Pa)
P	dimensionless pressure
Pr	Prandtl number
q_i''	total interfacial heat flux (W m^{-2})
Q_w	dimensionless local heat transfer through the wall
$\overline{Q_w}$	dimensionless average heat transfer through the wall
Ra	Rayleigh number
R_k	wall to nanofluid thermal conductivity ratio parameter
s	porous layer thickness (m)
S	dimensionless porous layer thickness
Sh	local Sherwood number
$\overline{\mathrm{Sh}}$	average Sherwood number
T	temperature (K)
u, v	velocity components along x, y directions, respectively (m s^{-1})
U, V	dimensionless velocity components along x, y directions, respectively
x, y	Cartesian coordinates (m)
X, Y	dimensionless Cartesian coordinates

Greek symbols

α	effective thermal diffusivity (m^2 s^{-1})
β	thermal expansion coefficient of the fluid (K^{-1})
Δ	difference value
ε	porosity of the porous medium
θ	dimensionless temperature
μ	dynamic viscosity (kg m^{-1} s^{-1})
ν	kinematic viscosity (m^2 s^{-1})
ρ	density (kg m^{-3})
(ρc)	effective heat capacity (J K^{-1} m^{-3})
τ	parameter defined by $\tau = (\rho c)_p/(\rho c)_{nf}$
ϕ	relative nanoparticle volume fraction
Ψ	dimensionless stream function

Subscripts

0	ambient property
c	cold
eff	effective
h	hot
max	maximum
nf	nanofluid
nff	nanofluid of free fluid layer
nfp	nanofluid of porous layer
p	nanoparticle
s	solid porous matrix
w	wall

the effect of porous layer on natural convection of a vertical cavity. The flow in porous region was simulated using Brinkman–Forchheimer-extended Darcy model. The results showed that high-permeable porous layer highly affects the natural convection patterns in the cavity. The degree of influence depends approximately on the product of Rayleigh and Darcy number. For values greater than 50, the effect of porous layer on natural convection is significant. Wu et al. [4] numerically analyzed the non-Darcy natural convection heat transfer in a 2D square cavity filled with a porous media. Uniform heat generation was considered inside the porous region. Half of the left and right walls of the cavity was maintained at lower temperature while the remaining sections were insulated. They studied the effects of cooling location and porous layer parameters such as Darcy number on the flow and thermal fields. Enhanced heat transfer rate was reported as the Darcy number increases.

The studies have shown that further heat transfer improvement can be achieved through adding high conductive nanosized particles to the fluid filling the porous media [5]. Bourantas et al. [6] performed a numerical investigation to study the natural convection in a porous cavity saturated by a nanofluid. A heat source was situated at the bottom wall of the container while the other walls were kept at a constant temperature. The results indicated an increase in Nusselt number as the solid volume fraction of nanoparticles increases. Chamkha and Ismael [7] considered the steady natural

convection in a square cavity totally filled with porous medium and saturated by a nanofluid. Heating was conducted through a triangular solid wall located at the lower left corner. It was found that the heat transfer may be strengthened or suppressed as the nanoparticle volume fraction varies. The trend will be determined by the Rayleigh number and triangular heating block thickness. In an experimental study by Solomon et al. [8], enhanced heat transfer was observed for nanofluid concentration less than 0.05% while the performance was deteriorated for greater concentrations. More studies investigating the natural convection in porous cavities saturated with nanofluids under different boundary and operating conditions can be found in the literature [9, 10].

The study of nanofluid-filled container is not limited to square cavities filled entirely with a porous medium. The porous layer can be placed vertically or horizontally inside the container. In another study, Chamkha and Ismael [11] demonstrated heat transfer enhancement in a nanofluid-saturated cavity by locating a vertical porous layer adjacent to the hot wall. It was reported that for the Rayleigh number less than 10^{-5}, Nusselt number will be maximum for a certain thickness of the porous layer. In a configuration presented by Al-Zamily [12], a vertical porous layer was positioned at the center of the cavity. The left wall was isothermally cooled while the right wall was partially heated. TiO_2–water was used as the nanofluid to saturate the clear and porous regions. The results showed higher heat transfer rate when the heat source was located at the bottom half of the left wall. They also presented that the average Nusselt number decreases as the Darcy number or the porous layer thickness increases.

Modeling of a composite problem including a porous medium and a clear region both saturated with nanofluid has its own complexities. A proper model should be able to describe the thermal fluid phenomena associated with the porous media and nanofluid as well as the interface between the two regions. Dating back in 1856, Darcy's law was introduced to describe the flow through porous medium where the fluid rate is proportional to the pressure drop and viscosity of the fluid [13]. However, the model was only generating acceptable results for low flow rates. As the flow rates increase, the flow does not obey the Darcy law due to the inertial and wall viscous forces. The deviations from the Darcy regime due to the abovementioned forces are generally referred to the non-Darcian effects. Forchheimer–Brinkman-extended Darcy model was proposed to overcome this issue [14]. The model has been adopted by some of the researchers to describe the natural convection in cavities filled totally or partially with porous materials [15–17].

There are two approaches to represent the heat transfer through a porous medium saturated with a liquid: the local thermal equilibrium (LTE) model and the local thermal nonequilibrium (LTNE) model. LTNE model accounts for the temperature difference between the solid and liquid phases in the porous matrix, while the LTE assumes LTE between the two phases [18]. The search in the literature shows that the LTE has been widely used to model natural convection in porous cavities [19–21]. However, it might fail to give accurate results for some specific conditions such as cases with low Biot number or when there is a significant difference between the thermal conductivities of the fluid and porous structure [18]. Baytas and Pop [22] utilized the LTNE model to investigate the natural convection heat transfer in a porous cavity. They reported that using such model modifies the flow behavior and heat transfer rates. Haddad et al. [23] investigated the validity of LTE assumption for natural convection near a vertical flat plate. They concluded that there are four parameters controlling the LTE assumption including Biot number, modified Darcy number, modified Rayleigh number, and dynamic viscosity ratio. Although LTNE plays an important role in thermal–fluid behavior of the porous enclosure, articles adopting this model when dealing with nanofluid in partial porous cavities are limited. Alsabery et al. [24] applied LTNE assumption to describe the natural convection in a nanofluid-saturated porous cavity. The left wall of the cavity was kept at a constant temperature, while the right wall was heated sinusoidally.

The interface between the porous region and the clear fluid plays a significant role in determination of convective heat transfer characteristics of the composite systems.

Several approaches have been proposed to describe the convective flow and heat transfer of nanofluids, including homogenous, dispersion, and Buongiorno model [25]. In homogenous

modeling, the nanofluid is assumed uniform with no slip between the base fluid and nanoparticles. The pure fluid equations are applied using thermophysical properties of the nanofluid [25]. Ghasemi and Siavashi [26] utilized homogenous model along with Forchheimer–Brinkman-extended Darcy equation to study the natural convection of nanofluid in square cavity with different boundary conditions.

Dispersion model has been developed assuming that enhanced heat transfer occurs because of the nanoparticle dispersion as well as the increased thermal conductivity. Using dispersion model, Shermet et al. [25] analyzed the transient natural convection in a wavy porous cavity.

Buongiorno developed a nonhomogeneous model incorporating the effects of Brownian diffusion and thermophoretic forces, that are proven to be important slip mechanisms in nanofluids [25]. Recently, the model proposed by Buongiorno has been applied to simulate nanofluid-free convection in porous cavities [27–30]. Yekani Motlagh et al. [29], using the Buongiorno model, investigated the natural convection of Al_2O_3–water and Cu–water in an inclined porous cavity. They studied the effects of porous matrix porosity, inclination angle of the enclosure, particle volume fraction, and porous Rayleigh numbers on the fluid flow and heat transfer rate.

To the author's knowledge, most of the available studies regarding the free convention in porous cavities saturated by nanofluids are limited to those the container is entirely filled with a porous media. Given the importance of cavities partially filled with a porous structure, this paper intends to explore the effects of nanoparticles on the fluid and thermal characteristics of such problems. The LTNE model is implemented to describe the heat transfer within the porous layer. The nanofluid is modeled using the Buongiorno's model to incorporate the thermophoresis and Brownian motion effects.

2. Mathematical formulation

Consider a steady, incompressible natural convection flow and heat transfer in a two-dimensional square cavity partially filled with a porous medium. As shown in Figure 1, the heat conducting solid wall with the thickness of d is considered at the left side. The isotropic and homogenous porous layer with a thickness s is saturated with a nanofluid, which also fills the remaining portion of the enclosure. The left vertical surface of the impermeable wall is at constant temperature T_h, while the right vertical surface of the cavity is kept at a constant temperature T_c. Horizontal walls are considered as adiabatic. All boundaries are assumed impermeable and nonslip boundary condition

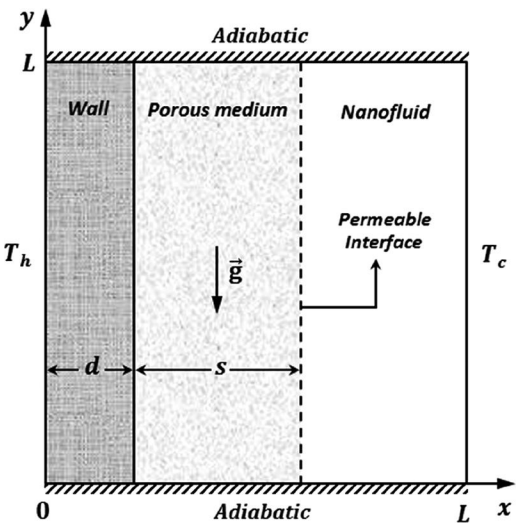

Figure 1. Schematic of the physical model and coordinate system.

is applied. In addition, it is assumed that the enclosure walls are impermeable to the nanoparticles; thus, the mass flux of nanoparticles is zero at the cavity walls. Furthermore, the nanoparticles are suspended in the nanofluid utilizing a surface charge technology or a surfactant. In fact, this prevents the nanoparticles from agglomeration on the solid porous matrix or agglutinating together [31, 32]. All thermophysical properties are assumed constant except for the density of nanofluid, which varies with temperature based on the Boussinesq approximation. It is also assumed that there is a LTE between the base fluid and the nanoparticles while the LTNE exists between the solid porous matrix and nanofluid. In the porous medium, the Brinkman–Forchheimer-extended Darcy model without the Forchheimer's inertia term has been adopted [3].

Considering all the abovementioned assumptions, the conservation equations for the total mass, momentum, thermal energy, and nanoparticles are represented for the nanofluid and porous domains as follow [13, 25, 31, 33–36]:

2.1. Nanofluid layer

$$\frac{\partial u}{\partial x}+\frac{\partial v}{\partial y}=0 \tag{1}$$

$$\rho_{nf}\left(u\frac{\partial u}{\partial x}+v\frac{\partial u}{\partial y}\right)=-\frac{\partial p}{\partial x}+\mu_{nf}\left(\frac{\partial^2 u}{\partial x^2}+\frac{\partial^2 u}{\partial y^2}\right) \tag{2}$$

$$\begin{aligned}\rho_{nf}\left(u\frac{\partial v}{\partial x}+v\frac{\partial v}{\partial y}\right)&=-\frac{\partial p}{\partial y}+\mu_{nf}\left(\frac{\partial^2 v}{\partial x^2}+\frac{\partial^2 v}{\partial y^2}\right)\\&+\left[-\left(\rho_{p,0}-\rho_{f,0}\right)(C-C_0)+(1-C_0)\rho_{f,0}\beta\left(T_{nf}-T_c\right)\right]g\end{aligned} \tag{3}$$

$$\begin{aligned}u\frac{\partial T_{nf}}{\partial x}+v\frac{\partial T_{nf}}{\partial y}&=\frac{k_{nf}}{(\rho c)_{nf}}\left(\frac{\partial^2 T_{nf}}{\partial x^2}+\frac{\partial^2 T_{nf}}{\partial y^2}\right)\\&+\tau\left\{D_B\left(\frac{\partial C}{\partial x}\frac{\partial T_{nf}}{\partial x}+\frac{\partial C}{\partial y}\frac{\partial T_{nf}}{\partial y}\right)+\frac{D_T}{T_c}\left[\left(\frac{\partial T_{nf}}{\partial x}\right)^2+\left(\frac{\partial T_{nf}}{\partial y}\right)^2\right]\right\}\end{aligned} \tag{4}$$

$$u\frac{\partial C}{\partial x}+v\frac{\partial C}{\partial y}=D_B\left(\frac{\partial^2 C}{\partial x^2}+\frac{\partial^2 C}{\partial y^2}\right)+\frac{D_T}{T_c}\left(\frac{\partial^2 T_{nf}}{\partial x^2}+\frac{\partial^2 T_{nf}}{\partial y^2}\right) \tag{5}$$

where u and v are the velocity components in x and y directions, respectively, C is the nanoparticle volume concentration, ρ is the density, T is the temperature, D_T is thermophoretic diffusion coefficient, D_B is the Brownian diffusion coefficient, and τ is defined as $(\rho c)_p/(\rho c)_{nf}$.

2.2. Porous layer

$$\frac{\partial u}{\partial x}+\frac{\partial v}{\partial y}=0 \tag{6}$$

$$\frac{\rho_{nf}}{\varepsilon^2}\left(u\frac{\partial u}{\partial x}+v\frac{\partial u}{\partial y}\right)=-\frac{\partial p}{\partial x}+\frac{\mu_{nf}}{\varepsilon}\left(\frac{\partial^2 u}{\partial x^2}+\frac{\partial^2 u}{\partial y^2}\right)-\frac{\mu_{nf}}{K}u \tag{7}$$

$$\frac{\rho_{nf}}{\varepsilon^2}\left(u\frac{\partial v}{\partial x}+v\frac{\partial v}{\partial y}\right)=-\frac{\partial p}{\partial y}+\frac{\mu_{nf}}{\varepsilon}\left(\frac{\partial^2 v}{\partial x^2}+\frac{\partial^2 v}{\partial y^2}\right)-\frac{\mu_{nf}}{K}v + \left[-\left(\rho_{p,0}-\rho_{f,0}\right)(C-C_0)+(1-C_0)\rho_{f,0}\beta\left(T_{nf}-T_c\right)\right]g \tag{8}$$

$$\frac{1}{\varepsilon}\left(u\frac{\partial T_{nf}}{\partial x}+v\frac{\partial T_{nf}}{\partial y}\right)=\alpha_{nf}\left(\frac{\partial^2 T_{nf}}{\partial x^2}+\frac{\partial^2 T_{nf}}{\partial y^2}\right)+\tau\left\{D_B\left(\frac{\partial C}{\partial x}\frac{\partial T_{nf}}{\partial x}+\frac{\partial C}{\partial y}\frac{\partial T_{nf}}{\partial y}\right) + \left(\frac{D_T}{T_c}\right)\left[\left(\frac{\partial T_{nf}}{\partial x}\right)^2+\left(\frac{\partial T_{nf}}{\partial y}\right)^2\right]\right\}+\frac{h_{nfs}\left(T_s-T_{nf}\right)}{\varepsilon(\rho c)_{nf}} \tag{9}$$

$$0=\alpha_s\left(\frac{\partial^2 T_s}{\partial x^2}+\frac{\partial^2 T_s}{\partial y^2}\right)+\frac{h_{nfs}}{(1-\varepsilon)(\rho c)_s}\left(T_{nf}-T_s\right) \tag{10}$$

$$\frac{1}{\varepsilon}\left(u\frac{\partial C}{\partial x}+v\frac{\partial C}{\partial y}\right)=D_B\left(\frac{\partial^2 C}{\partial x^2}+\frac{\partial^2 C}{\partial y^2}\right)+\left(\frac{D_T}{T_c}\right)\left(\frac{\partial^2 T_{nf}}{\partial x^2}+\frac{\partial^2 T_{nf}}{\partial y^2}\right) \tag{11}$$

where $\tau=(\rho c)_p/(\rho c)_{nf}$.

2.3. Wall layer

The energy equation for the impermeable wall layer is:

$$\frac{\partial^2 T_w}{\partial x^2}+\frac{\partial^2 T_w}{\partial y^2}=0 \tag{12}$$

3. Interface boundary conditions

3.1. Free nanofluid–porous interface

Several researches on the proper fluid–porous interface boundary conditions for the fluid flow and heat transfer phenomena have been performed [34, 37–40]. In the present study, the continuities of velocity and stress are considered. Moreover, continuous temperature is assumed at the interface between the nanofluid and porous regions [37, 40]:

$$\begin{aligned} u_{\text{free nanofluid}} &= u_{\text{porous}} \quad , \quad v_{\text{free nanofluid}} = v_{\text{porous}} \\ \mu_{nf}\left.\frac{\partial u}{\partial x}\right|_{\text{free nanofluid}} &= \mu_{nf,\text{eff}}\left.\frac{\partial u}{\partial x}\right|_{\text{porous}} \quad , \quad \mu_{nf}\left.\frac{\partial v}{\partial x}\right|_{\text{free nanofluid}} = \mu_{nf,\text{eff}}\left.\frac{\partial v}{\partial x}\right|_{\text{porous}} \\ T_{nf}\big|_{\text{free nanofluid}} &= T_{nf}\big|_{\text{porous}} = T_s\big|_{\text{porous}} \\ k_{nf}\left.\frac{\partial T_{nf}}{\partial x}\right|_{\text{free nanofluid}} &= k_{nf,\text{eff}}\left.\frac{\partial T_{nf}}{\partial x}\right|_{\text{porous}} + k_{s,\text{eff}}\left.\frac{\partial T_s}{\partial x}\right|_{\text{porous}} = q_i'' \\ C_{\text{free nanofluid}} &= C_{\text{porous}} \quad , \quad \left.\frac{\partial C}{\partial x}\right|_{\text{free nanofluid}} = \left.\frac{\partial C}{\partial x}\right|_{\text{porous}} \end{aligned} \tag{13}$$

Here q_i'' is the total interfacial heat flux, which characterizes the heat transfer through the porous region. In addition, the effective thermal conductivity of the nanofluid and solid matrix can be expressed by $k_{nf,\text{eff}}=\varepsilon k_{nf}$ and $k_{s,\text{eff}}=(1\text{-}\varepsilon)k_s$, respectively. It is worth mentioning that due to utilizing nanofluid in the enclosure, the interfacial heat transfer between the fluid and the solid phases is high enough; therefore, considering the fluid and solid temperatures at the interface to be identical seems reasonable [41].

3.2. Wall–porous interface

The boundary conditions for the velocity and the pressure fields at the interface of a pure solid domain and a porous region are well known and are similar to the conditions that are generally applied at impermeable boundaries. The typical no-slip and no-penetration conditions are utilized for the velocity at the interface, while the pressure is simply obtained by extrapolation using the porous domain interior pressure values.

Considering continuous temperature distribution and using energy balance at the interface, the corresponding thermal boundary conditions at the interface between the wall and porous regions can be written as [40, 42]:

$$\begin{aligned} & T_w|_{\text{wall}} = T_{nf}\big|_{\text{porous}} = T_{\text{s}}|_{\text{porous}} \\ & k_w \frac{\partial T_w}{\partial x}\bigg|_{\text{wall}} = k_{nf,\text{eff}} \frac{\partial T_{nf}}{\partial x}\bigg|_{\text{porous}} + k_{s,\text{eff}} \frac{\partial T_{\text{s}}}{\partial x}\bigg|_{\text{porous}} = q_i'' \\ & D_{\text{B}} \frac{\partial C}{\partial x}\bigg|_{\text{porous}} + \frac{D_T}{T_c} \frac{\partial T_{nf}}{\partial x}\bigg|_{\text{porous}} = 0 \end{aligned} \tag{14}$$

4. Dimensionless equations

To nondimensionalize Eqs. (1)–(14), the dimensional variables are scaled utilizing the following dimensionless parameters:

$$\begin{aligned} & X = \frac{x}{L}, Y = \frac{y}{L}, D = \frac{d}{L}, S = \frac{s}{L}, U = \frac{uL}{\alpha_{nf}}, V = \frac{vL}{\alpha_{nf}}, P = \frac{pL^2}{\rho_{nf}\alpha_{nf}^2}, \\ & \text{Pr} = \frac{\nu_{nf}}{\alpha_{nf}}, \text{Da} = \frac{K}{L^2}, \phi = \frac{C}{C_0}, \text{Ra} = \frac{(1-C_0)\rho_{f,0} g\beta\,\Delta T L^3}{\alpha_{nf}\mu_{nf}}, \\ & \theta_{nf} = \left(T_{nf} - T_{\text{c}}\right)/\Delta T, \theta_{\text{s}} = \left(T_{\text{s}} - T_{\text{c}}\right)/\Delta T, \theta_w = \left(T_w - T_{\text{c}}\right)/\Delta T, \\ & \text{Nr} = \frac{\left(\rho_{p,0} - \rho_{f,0}\right)C_0}{\rho_{f,0}\beta\,\Delta T(1-C_0)}, \quad \text{Nb} = \frac{\tau D_{\text{B}} C_0}{\alpha_{nf}}, \text{Nt} = \frac{\tau D_{\text{T}}\Delta T}{\alpha_{nf}\,T_{\text{c}}}, \\ & H = \frac{h_{nfs}L^2}{k_{nf}}, K_r = \frac{k_{nf}}{(1-\varepsilon)k_{\text{s}}}, \text{Le} = \frac{\alpha_{nf}}{D_{\text{B}}}, R_k = \frac{k_w}{k_{nf}} \end{aligned} \tag{15}$$

where $\Delta T = T_h - T_{\text{c}}$.

Consequently, by substituting the introduced dimensionless parameters into Eqs. (1)–(14), the nondimensional governing equations and boundary conditions can be written as:

4.1. Nanofluid layer

$$\frac{\partial U}{\partial X} + \frac{\partial V}{\partial Y} = 0 \tag{16}$$

$$U\frac{\partial U}{\partial X} + V\frac{\partial U}{\partial Y} = -\frac{\partial P}{\partial X} + \text{Pr}\left(\frac{\partial^2 U}{\partial X^2} + \frac{\partial^2 U}{\partial Y^2}\right) \tag{17}$$

$$U\frac{\partial V}{\partial X} + V\frac{\partial V}{\partial Y} = -\frac{\partial P}{\partial Y} + \text{Pr}\left(\frac{\partial^2 V}{\partial X^2} + \frac{\partial^2 V}{\partial Y^2}\right) - \text{Ra}\cdot\text{Pr}\cdot\text{Nr}(\phi - 1) + \text{Ra}\cdot\text{Pr}\cdot\theta_{nf} \tag{18}$$

$$U\frac{\partial \theta_{nf}}{\partial X} + V\frac{\partial \theta_{nf}}{\partial Y} = \frac{\partial^2 \theta_{nf}}{\partial X^2} + \frac{\partial^2 \theta_{nf}}{\partial Y^2} + \text{Nb}\left(\frac{\partial \phi}{\partial X}\frac{\partial \theta_{nf}}{\partial X} + \frac{\partial \phi}{\partial Y}\frac{\partial \theta_{nf}}{\partial Y}\right) + \text{Nt}\left[\left(\frac{\partial \theta_{nf}}{\partial X}\right)^2 + \left(\frac{\partial \theta_{nf}}{\partial Y}\right)^2\right] \tag{19}$$

$$U\frac{\partial \phi}{\partial X}+V\frac{\partial \phi}{\partial Y}=\frac{1}{\mathrm{Le}}\left(\frac{\partial^2 \phi}{\partial X^2}+\frac{\partial^2 \phi}{\partial Y^2}\right)+\frac{\mathrm{Nt}}{\mathrm{Le}\cdot \mathrm{Nb}}\left(\frac{\partial^2 \theta_{nf}}{\partial X^2}+\frac{\partial^2 \theta_{nf}}{\partial Y^2}\right) \tag{20}$$

4.2. Porous layer

$$\frac{\partial U}{\partial X}+\frac{\partial V}{\partial Y}=0 \tag{21}$$

$$\frac{1}{\varepsilon^2}\left(U\frac{\partial U}{\partial X}+V\frac{\partial U}{\partial Y}\right)=-\frac{\partial P}{\partial X}+\frac{\mathrm{Pr}}{\varepsilon}\left(\frac{\partial^2 U}{\partial X^2}+\frac{\partial^2 U}{\partial Y^2}\right)-\frac{\mathrm{Pr}}{\mathrm{Da}}U \tag{22}$$

$$\frac{1}{\varepsilon^2}\left(U\frac{\partial V}{\partial X}+V\frac{\partial V}{\partial Y}\right)=-\frac{\partial P}{\partial Y}+\frac{\mathrm{Pr}}{\varepsilon}\left(\frac{\partial^2 V}{\partial X^2}+\frac{\partial^2 V}{\partial Y^2}\right)-\frac{\mathrm{Pr}}{\mathrm{Da}}V-\mathrm{Ra}\cdot\mathrm{Pr}\cdot\mathrm{Nr}(\phi-1)+\mathrm{Ra}\cdot\mathrm{Pr}\cdot\theta_{nf} \tag{23}$$

$$\begin{aligned}U\frac{\partial \theta_{nf}}{\partial X}+V\frac{\partial \theta_{nf}}{\partial Y}&=\varepsilon\left(\frac{\partial^2 \theta_{nf}}{\partial X^2}+\frac{\partial^2 \theta_{nf}}{\partial Y^2}\right)+\mathrm{Nb}\cdot\varepsilon\left(\frac{\partial \phi}{\partial X}\frac{\partial \theta_{nf}}{\partial X}+\frac{\partial \phi}{\partial Y}\frac{\partial \theta_{nf}}{\partial Y}\right)\\&\quad+\mathrm{Nt}\cdot\varepsilon\left[\left(\frac{\partial \theta_{nf}}{\partial X}\right)^2+\left(\frac{\partial \theta_{nf}}{\partial Y}\right)^2\right]+H\left(\theta_s-\theta_{nf}\right)\end{aligned} \tag{24}$$

$$0=\frac{\partial^2 \theta_s}{\partial X^2}+\frac{\partial^2 \theta_s}{\partial Y^2}+H\cdot K_r\left(\theta_{nf}-\theta_s\right) \tag{25}$$

$$U\frac{\partial \phi}{\partial X}+V\frac{\partial \phi}{\partial Y}=\frac{\varepsilon}{\mathrm{Le}}\left(\frac{\partial^2 \phi}{\partial X^2}+\frac{\partial^2 \phi}{\partial Y^2}\right)+\frac{\mathrm{Nt}\cdot\varepsilon}{\mathrm{Le}\cdot\mathrm{Nb}}\left(\frac{\partial^2 \theta_{nf}}{\partial X^2}+\frac{\partial^2 \theta_{nf}}{\partial Y^2}\right) \tag{26}$$

4.3. Wall layer

$$\frac{\partial^2 \theta_w}{\partial X^2}+\frac{\partial^2 \theta_w}{\partial Y^2}=0 \tag{27}$$

4.4. Nondimensional interfacial boundary conditions

4.4.1. Nanofluid–porous interface

$$\begin{aligned}U_{\text{free nanofluid}}&=U_{\text{porous}}\quad,\quad V_{\text{free nanofluid}}=V_{\text{porous}}\\\left.\frac{\partial U}{\partial X}\right|_{\text{free nanofluid}}&=\frac{1}{\varepsilon}\left.\frac{\partial U}{\partial X}\right|_{\text{porous}}\quad,\quad\left.\frac{\partial V}{\partial X}\right|_{\text{free nanofluid}}=\frac{1}{\varepsilon}\left.\frac{\partial V}{\partial X}\right|_{\text{porous}}\\\theta_{nf}\big|_{\text{free nanofluid}}&=\theta_{nf}\big|_{\text{porous}}=\theta_s\big|_{\text{porous}}\\\left.\frac{\partial \theta_{nf}}{\partial X}\right|_{\text{free nanofluid}}&=\varepsilon\left.\frac{\partial \theta_{nf}}{\partial X}\right|_{\text{porous}}+K_r^{-1}\left.\frac{\partial \theta_s}{\partial X}\right|_{\text{porous}}=\frac{q_i''L}{k_{nf}\Delta T}=Q_i\\\phi_{\text{free nanofluid}}&=\phi_{\text{porous}}\quad,\quad\left.\frac{\partial \phi}{\partial X}\right|_{\text{free nanofluid}}=\left.\frac{\partial \phi}{\partial X}\right|_{\text{porous}}\end{aligned} \tag{28}$$

4.4.2. Wall–porous interface

$$\begin{aligned}
&\theta_w|_{\text{wall}} = \theta_{nf}\big|_{\text{porous}} = \theta_s|_{\text{porous}} \\
&R_k \frac{\partial \theta_w}{\partial X}\bigg|_{\text{wall}} = \varepsilon \frac{\partial \theta_{nf}}{\partial X}\bigg|_{\text{porous}} + K_r^{-1} \frac{\partial \theta_s}{\partial X}\bigg|_{\text{porous}} = \frac{q_i'' L}{k_{nf} \Delta T} = Q_i \\
&\text{Nb} \frac{\partial \phi}{\partial X}\bigg|_{\text{porous}} + \text{Nt} \frac{\partial \theta_{nf}}{\partial X}\bigg|_{\text{porous}} = 0
\end{aligned} \tag{29}$$

Furthermore, the other dimensionless boundary conditions on the vertical and horizontal walls can be written as:

$$\begin{aligned}
&\theta_w(0, Y) = 1 \\
&U(1, Y) = V(1, Y) = 0, \quad \theta_{nf}(1, Y) = 0, \quad \text{Nb} \frac{\partial \phi(1, Y)}{\partial X} + \text{Nt} \frac{\partial \theta_{nf}(1, Y)}{\partial X} = 0 \\
&U(X, 0) = V(X, 0) = 0, \quad \frac{\partial \theta_w(X, 0)}{\partial Y} = \frac{\partial \theta_{nf}(X, 0)}{\partial Y} = \frac{\partial \theta_s(X, 0)}{\partial Y} = 0, \quad \frac{\partial \phi(X, 0)}{\partial Y} = 0 \\
&U(X, 1) = V(X, 1) = 0, \quad \frac{\partial \theta_w(X, 1)}{\partial Y} = \frac{\partial \theta_{nf}(X, 1)}{\partial Y} = \frac{\partial \theta_s(X, 1)}{\partial Y} = 0, \quad \frac{\partial \phi(X, 1)}{\partial Y} = 0
\end{aligned} \tag{30}$$

The physical quantities of interest in this problem are the heat transfer through the wall Q_w, the local Nusselt numbers Nu_{nfp}, Nu_s, Nu_{nff}, the local Sherwood number Sh, the average heat transfer through the wall $\overline{Q_w}$, and the average Nusselt $\overline{\text{Nu}_{nfp}}$, $\overline{\text{Nu}_s}$, $\overline{\text{Nu}_{nff}}$, and Sherwood $\overline{\text{Sh}}$ numbers, which are defined as below:

$$\begin{aligned}
Q_w &= \left(-\frac{\partial \theta_w}{\partial X} \right)_{X=0,D} \\
\text{Nu}_{nfp} = \left(-\frac{\partial \theta_{nf}}{\partial X} \right)_{X=D,D+S}&, \text{Nu}_s = \left(-\frac{\partial \theta_s}{\partial X} \right)_{X=D,D+S}, \text{Nu}_{nff} = \left(-\frac{\partial \theta_{nf}}{\partial X} \right)_{X=D+S,1} \\
\text{Sh} &= \left(-\frac{\partial \phi}{\partial X} \right)_{X=D,D+S}
\end{aligned} \tag{31}$$

$$\overline{Q_w} = \int_0^1 Q_w \, \mathrm{d}Y, \overline{\text{Nu}} = \int_0^1 \text{Nu} \, \mathrm{d}Y, \overline{\text{Sh}} = \int_0^1 \text{Sh} \, \mathrm{d}Y \tag{32}$$

where Nu_{nfp}, Nu_s, and Nu_{nff} denote the Nusselt number of the nanofluid in the porous layer, the Nusselt number of the porous matrix in the porous layer, and the Nusselt number of the nanofluid in the free nanofluid, respectively.

It should be mentioned that based on the conservation of energy, $\text{Nu}_{ffp} = \left| \left(-\frac{\partial \theta_{nf}}{\partial X} \right)_{X=D+S} \right| = \left| \left(-\frac{\partial \theta_{nf}}{\partial X} \right)_{X=1} \right|$ and $Q_w = \left| \left(-\frac{\partial \theta_w}{\partial X} \right)_{X=0} \right| = \left| \left(-\frac{\partial \theta_w}{\partial X} \right)_{X=D} \right|$. Therefore, in the present study, Nu_{nff} values are calculated at $X = D + S$.

Furthermore, using Eqs. (28) and (29), the following relationships between the average Nusselt numbers at the wall–porous and nanofluid–porous interfaces are obtained:

$$\overline{Q_w} = \varepsilon R_k^{-1} \overline{\text{Nu}_{nfp}} + R_k^{-1} K_r^{-1} \overline{\text{Nu}_s} \tag{33}$$

$$\overline{\text{Nu}_{nff}} = \varepsilon \overline{\text{Nu}_{nfp}} + K_r^{-1} \overline{\text{Nu}_s} \tag{34}$$

The streamlines are one of the best options to visualize the convective fluid flow structure inside the cavity, therefore; the nondimensional stream function Ψ is calculated as:

$$U = \frac{\partial \Psi}{\partial X}, V = -\frac{\partial \Psi}{\partial Y} \tag{35}$$

To calculate the Sherwood number values, it should be noted that at the vertical walls, the temperature gradient and the concentration gradients are linked as:

$$\frac{\partial \phi}{\partial X} = -\frac{\mathrm{Nt}}{\mathrm{Nb}} \frac{\partial \theta_{nf}}{\partial X} \tag{36}$$

Using Eq. (36), the local and average Sherwood numbers can be expressed as $\mathrm{Sh} = -\frac{\mathrm{Nt}}{\mathrm{Nb}}\mathrm{Nu}$ and $\overline{\mathrm{Sh}} = -\frac{\mathrm{Nt}}{\mathrm{Nb}}\overline{\mathrm{Nu}}$.

5. Numerical method and validation

To solve Eqs. (16)–(27) along with the corresponding boundary conditions given in Eqs. (28)–(30), they are transformed to a weak form and solved using the Galerkin finite element method [18, 43]. The Newton–Raphson method is utilized to fully couple the governing discretized equations [44]. The detailed solution procedure is given in the earlier literatures [45–49]. The iteration process is terminated when the following convergence condition for the dependent variables between two iterations is satisfied:

$$\frac{\sum \left| \kappa_{i,j}^{m+1} - \kappa_{i,j}^{m} \right|}{\sum \left| \kappa_{i,j}^{m+1} \right|} \leq 5 \times 10^{-3} \tag{36}$$

where κ stands for any dependent variable, such as θ_{nf}, θ_s, θ_w, U, V, or ϕ and m indicate the iteration step.

To obtain a grid-independent solution, a grid independency test is conducted considering five different sizes as shown in Table 1. The results obtained for average Nusselt numbers of the various phases and the average heat transfer through the wall are presented for each gird size. It should be noted that finer grids are generated near the boundaries, where large gradients of velocity and temperature are expected. Consequently, by considering both the accuracy and computational cost, the grid size of 100×100 is adopted for all the analysis.

To ensure the validity of the mathematical formulation, the results are compared to two different test cases. The first test case is the natural convection heat transfer within a porous layer saturated with pure fluid and is sandwiched between two equal thickness walls considering LTNE condition [42]. The second case is based on the study of Sheremet and Pop [27], where the natural convection heat transfer in a cavity with thick vertical walls is analyzed. The cavity is filled with a porous material and is saturated with a nanofluid.

Figures 2 and 3 show the isotherms, streamlines, and the average Nusselt numbers of the current study compared to the numerical results presented by Saeid [42]. In addition, Table 2 shows the amount of heat transfer through the walls, the average Nusselt number of the fluid and solid phases of the porous medium as well as the maximum stream function value for different thermal conductivity ratios in comparison with those presented by Saied [42]. For the second test case [27], the

Table.1. Grid independence test for $\mathrm{Ra} = 10^4$, $\mathrm{Da} = 10^{-2}$, $P_r = 5$, $\varepsilon = 0.6$, $\mathrm{Nr} = 10$, $\mathrm{Nb} = 10^{-6}$, $\mathrm{Nt} = 10^{-6}$, $\mathrm{Le} = 10^3$, $D = 0.1$, $S = 0.45$, $H = 10$, $K_r = 10$, and $R_k = 10$.

Grid size	$\overline{Q_w}$	$\overline{\mathrm{Nu}_{nfp}}$	$\overline{\mathrm{Nu}_{nfp}}$	$\overline{\mathrm{Nu}_{nff}}$
60×60	0.1583	2.3059	1.9962	1.5834
80×80	0.1585	2.3086	1.9974	1.5851
100×100	0.1586	2.3098	1.9980	1.5858
120×120	0.1586	2.3103	1.9982	1.5862
140×140	0.1586	2.3107	1.9984	1.5863

comparative results of the streamlines, isotherms, isoconcentrations, and the computed local Nusselt number at the wall–porous interface are shown in Figures 4 and 5.

As is seen in Figures 2–5 and Table 2, the obtained results of the current study are in good agreement with those reported by Saeid [42] and Sheremet and Pop [27] for both test cases.

6. Results and discussion

In this section, the obtained numerical results are presented in the form of isotherms and streamline contours and heat transfer characteristic graphs (Nusselt number). In addition, the effects of varying dimensionless parameters on the concentration contours (isoconcentrations) are reported. The analyses are performed for the following range of the associated dimensionless parameters; Rayleigh number ($10^3 \leq \mathrm{Ra} \leq 10^5$), Darcy number ($10^{-5} \leq \mathrm{Da} \leq 10^{-1}$), Prandtl number ($5 \leq \mathrm{Pr} \leq 1000$), porosity ($0.3 \leq \varepsilon \leq 0.9$), buoyancy ratio parameter ($0 \leq \mathrm{Nr} \leq 30$), Brownian motion parameter ($10^{-6} \leq \mathrm{Nb} \leq 10^{-4}$), thermophoresis parameter ($10^{-6} \leq \mathrm{Nt} \leq 10^{-4}$), Lewis number ($\mathrm{Le} = 10^3$), wall thickness to height ratio ($0.01 \leq D \leq 0.4$), porous layer thickness to height ratio ($0.2 \leq S \leq 0.8$), interface heat transfer coefficient ($0.1 \leq H \leq 1000$), thermal conductivity ratio for the porous medium ($1 \leq K_r \leq 100$), and the wall to nanofluid thermal conductivity ratio ($0.1 \leq R_k \leq 10$).

Figures 6–8 show the isotherms, streamlines, and isoconcentrations at different values of the considered dimensionless parameters. To study the problem in more detail, the values of average heat transfer through the wall, average Nusselt number of the nanofluid and solid phases of the porous layer as well as the Nusselt number of the nanofluid in the free layer, the absolute maximum stream function, and the maximum concentration of nanoparticles are presented here. An overview of the contour maps regardless of the studied parameter values reveals that there is a significant difference between the isotherms of the nanofluid and solid phase of the porous medium. Furthermore, a single clockwise convective rotating cell of the flow is formed inside the enclosure. In addition, according to the isoconcentrations, the nanoparticle concentration near the hot vertical wall–porous interface is low, while it is high near the cold vertical boundary. This is due to the fact that the thermophoresis forces are proportional to the temperature gradient, from hot to cold [35]. In fact, the thermophoresis forces cause the nanoparticles to migrate from the hot boundaries to the cold ones. The weakest and strongest concentrations of the nanoparticles occur at the top left corner and the bottom right corner of the enclosure, respectively. Furthermore, the isoconcentration contours display a thin concentration boundary layer with high concentration gradient of nanoparticles along the hot and cold vertical boundaries, whereas the concentration of nanoparticles is almost uniform in the core region of the enclosure. To clarify the cause of such a thin boundary layer formation, it should be referred to the definition of Lewis number. The Lewis number represents the ratio of thermal diffusivity to

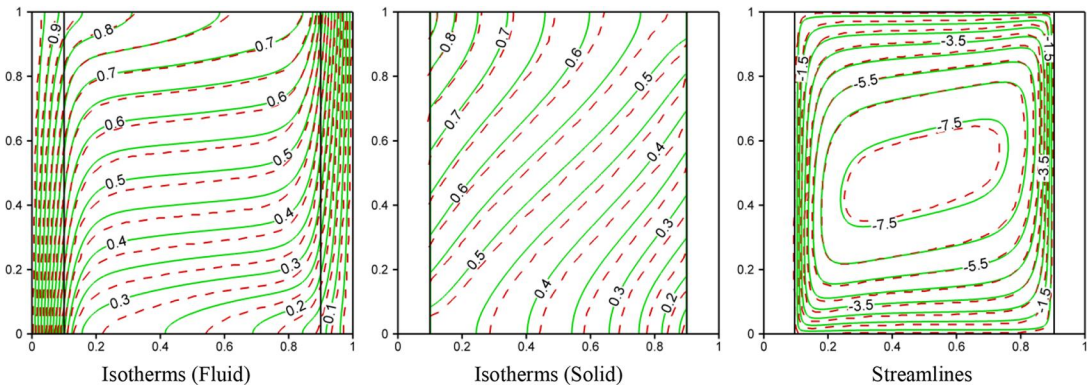

Figure 2. A comparison between the present study result (solid green line) and the results reported by Saeid [42] (dashed red line) for $\mathrm{Ra} = 10^3$, $D = 0.1$, $K_r = 10$, $R_k = 1$, $H = 1$, and $\Delta\theta = 0.05$.

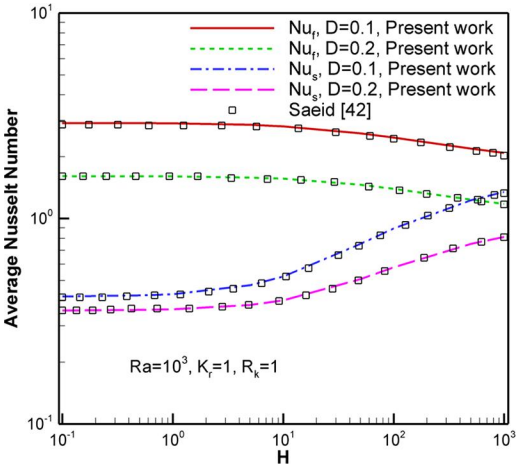

Figure 3. Variation of $\overline{Nu_f}$ and $\overline{Nu_s}$ of the present work and Saeid [42] with H for different values of D.

nanoparticle diffusion coefficient in nanofluids. The Brownian coefficient for diffusion of nanoparticles in comparison to the thermal diffusivity is very low, which leads to a large Lewis number. On the other hand, in terms of boundary layer theory, two different boundary layers are formed near the walls corresponding to the thermal diffusivity and the nanoparticle diffusion. Accordingly, the Lewis number can be considered as the ratio of thermal boundary layer thickness to the thickness of concentration boundary layer. The thickness of thermal boundary layer is nearly constant, which is mainly affected by the hydrodynamic boundary layer and the buoyancy forces. Hence, as a result of large values of the Lewis number, the concentration boundary layer of nanofluid is very thin.

As is observed in Figure 6*a* and *b*, by increasing the wall thickness, the average Nusselt numbers decrease and the isotherms slightly tend to be vertical, which indicates conduction dominant heat transfer in the enclosure. In addition, the strength of the single-cell circulation as well as the convection mode of heat transfer becomes weaker as indicated by the lower values of absolute maximum stream function. It is worth mentioning that the influence of thermophoresis phenomenon increases in the conduction dominant regime [50], thus, the concentration gradient of nanoparticles enhances with the increase in wall thicknesses in the vicinity of the boundaries.

The effect of porous layer thickness on the convective heat and mass transfer inside the enclosure is illustrated in Figure 6*a* and *c*. It can be observed that the strength of the rotational flow of nanofluid significantly increases as the porous layer thickness decreases. This behavior is due to the weakening of the hydrodynamic resistance of the porous region. The significant increase in the value of absolute stream function and the density of streamlines confirms the aforementioned behavior. It can also be noted that for the thick porous layer, the rotational cell is vertically elongated, whereas a circular cell is obtained for the thin porous layer case. The average Nusselt numbers increase with the decrease in

Table 2. Comparison of the present results with those by Saeid [42].

	$\mathrm{Ra} = 10^3, D = 0.1, K_r = 1, H = 1$				
	R_k	$\overline{Nu_f}$	$\overline{Nu_s}$	$\overline{Q_w}$	$\lvert\Psi\rvert_{max}$
Present results	0.1	0.343	0.112	4.557	3.635
	1	2.904	0.429	3.333	8.156
	10	9.840	1.013	1.085	16.029
Saeid [42]	0.1	0.326	0.110	4.357	3.536
	1	2.814	0.418	3.232	7.898
	10	9.887	1.010	1.090	16.219

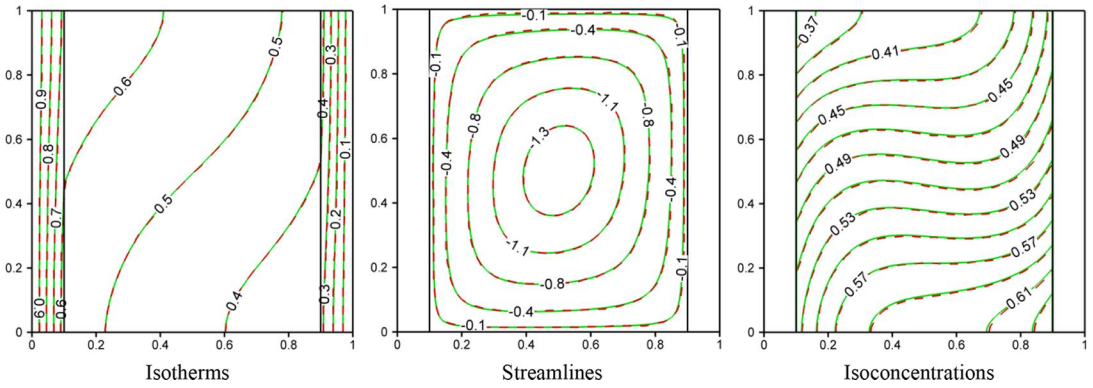

Figure 4. A comparison between the results of present study (solid green line) and the result reported by Sheremet and Pop [27] (dashed red line) in the case of Ra = 100, Le = 1, $K = 0.1$, $D = 0.1$, Nr = Nb = Nt = 0.1.

porous layer thickness. This is due to the increase in horizontal temperature gradient in the porous region. In accordance with Figure 6*c*, the shapes of the isotherms of the nanofluid and solid matrix in the porous region are almost identical. The similarity can be justified referring to the enhancement of thermal communication between the two phases, which is caused by intensification of the nanofluid flow velocity. Hence, implementing thermal equilibrium model seems appropriate under such circumstances.

Increasing each of the Darcy or Rayleigh numbers (Figures 6*a*, 7*a* and *b*) favors the nanofluid to flow more through the porous layer, so the intensity of convection and, consequently, average Nusselt number increases. In fact, the Darcy number indicates the permeability of the porous layer. Therefore, by increasing the Darcy number, more nanofluid is allowed to infiltrate the porous layer and as a result, the strengthe of the flow circulation significantly increases. In addition, the tendency of the isotherms of Figure 7*a* and *b* to the horizontal positon in comparsion with Figure 6*a* indicates the domination of convection mode in the enclosure especially within the free nanofluid layer.

Increase in the interface heat transfer coefficient between the nanofluid and solid porous matrix (H) (Figure 7*a* and *c*) leads to the decrease in the average Nusselt number of the nanofluid and the increase in the average Nusselt number of the solid matrix. In essence, the increase in the interface

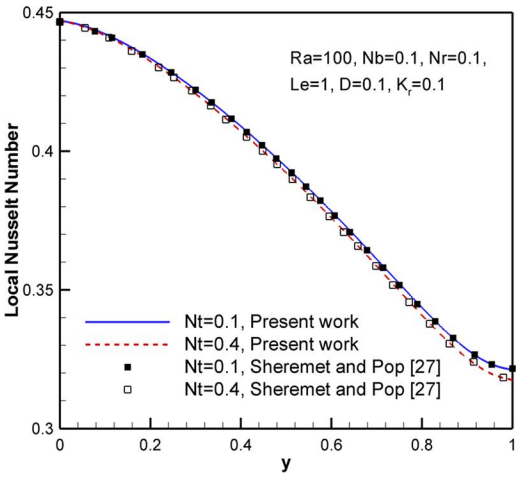

Figure 5. Variation of local Nusselt number at wall–porous interface ($x = D$) of the present work and Sheremet and Pop [27] for different values of Nt.

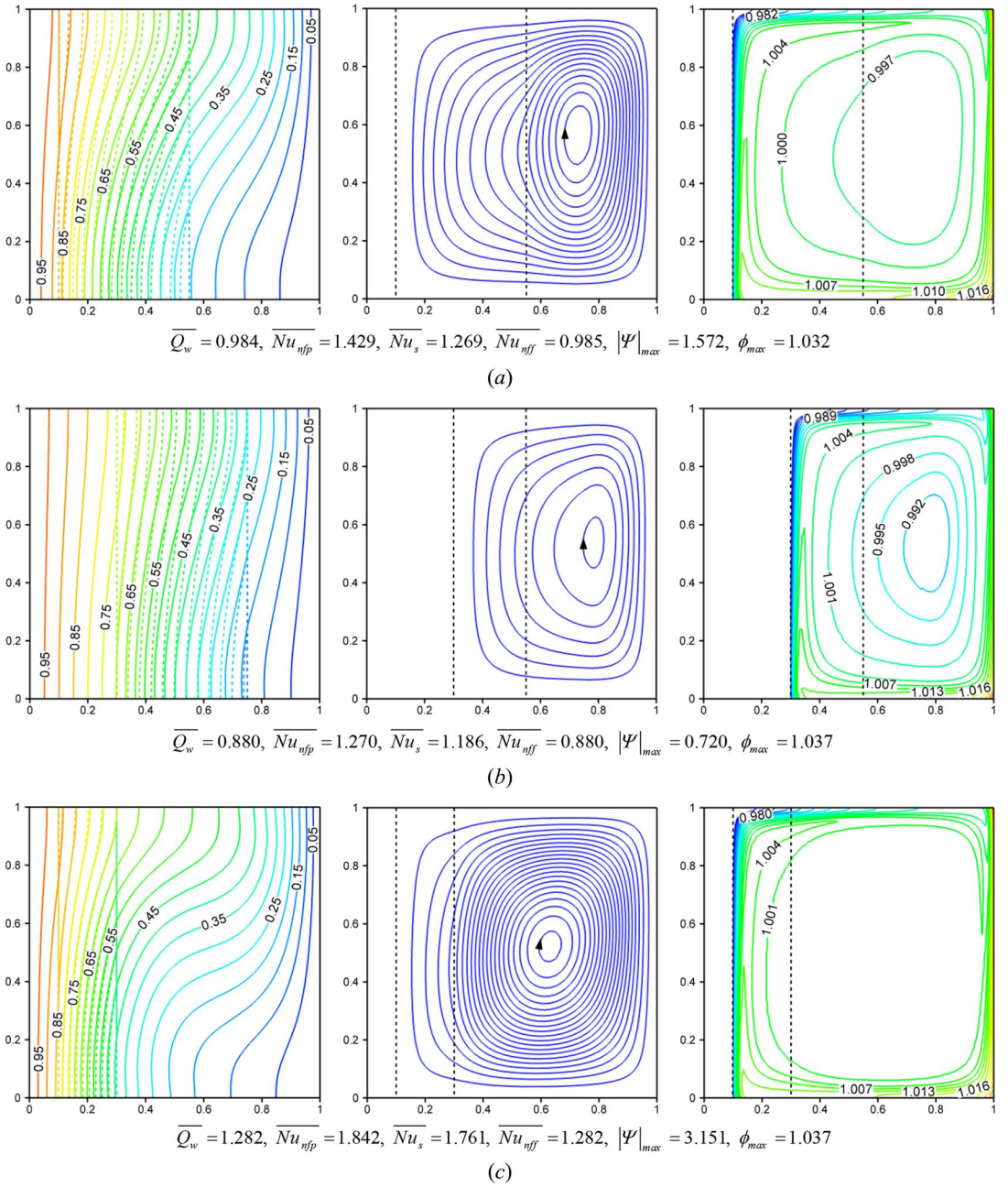

Figure 6. Isotherms (left) (solid line for θ_{nf}, dashed line for θ_s), streamlines (middle), and isoconcentrations (right) for $Ra = 10^4$, $Da = 10^{-3}$, $Pr = 5$, $Nr = 10$, $Nb = 10^{-6}$, $Nt = 10^{-6}$, $Le = 10^3$, $H = 1$, $K_r = 10$, $R_k = 1$, $\varepsilon = 0.6$: a) $D = 0.1$, $S = 0.45$, b) $D = 0.3$, $S = 0.45$, c) $D = 0.1$, $S = 0.2$.

heat transfer coefficient increases the thermal communications between the two phases of the porous medium. The temperature of the nanofluid rises while the solid porous matrix temperature reduces. Therefore, the temperature difference between the nanofluid and the hot wall drops, hence the average Nusselt number of the nanofluid decreases. Subsequently in reverse, the temperature difference between the solid porous matrix and the hot wall increases. This leads to the enhancement of the solid

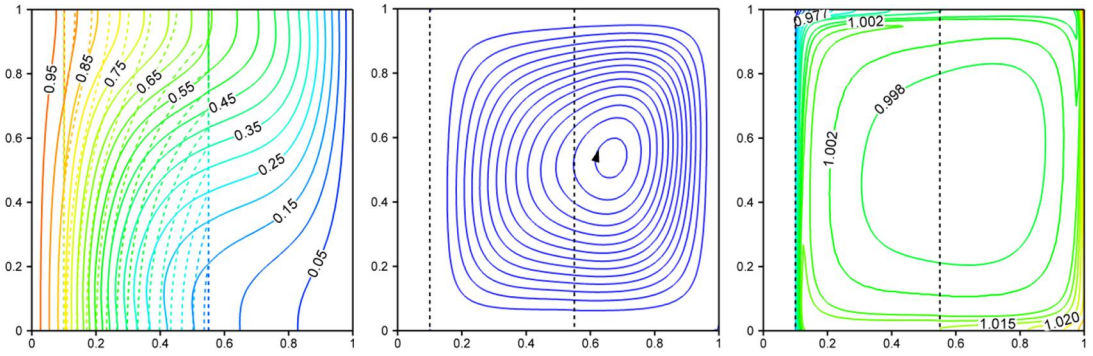

$\overline{Q_w} = 1.336,\ \overline{Nu_{nfp}} = 2.006,\ \overline{Nu_s} = 1.319,\ \overline{Nu_{nff}} = 1.336,\ |\Psi|_{max} = 2.863,\ \phi_{max} = 1.042$

(*a*)

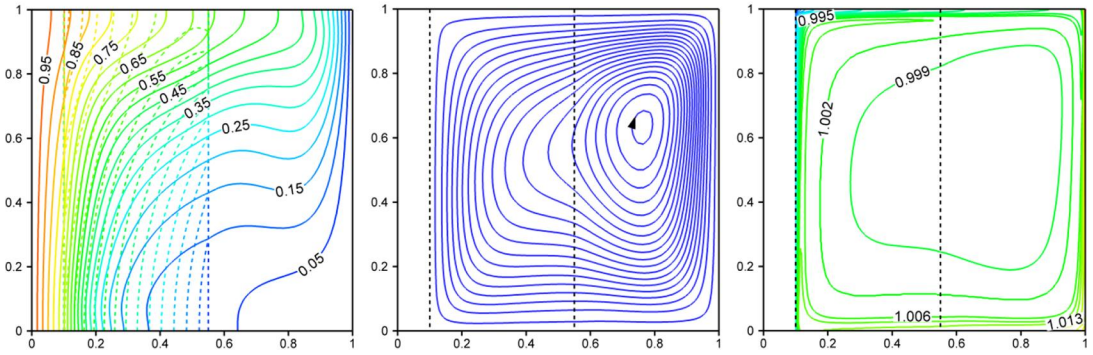

$\overline{Q_w} = 2.012,\ \overline{Nu_{nfp}} = 3.113,\ \overline{Nu_s} = 1.444,\ \overline{Nu_{nff}} = 2.012,\ |\Psi|_{max} = 5.581,\ \phi_{max} = 1.037$

(*b*)

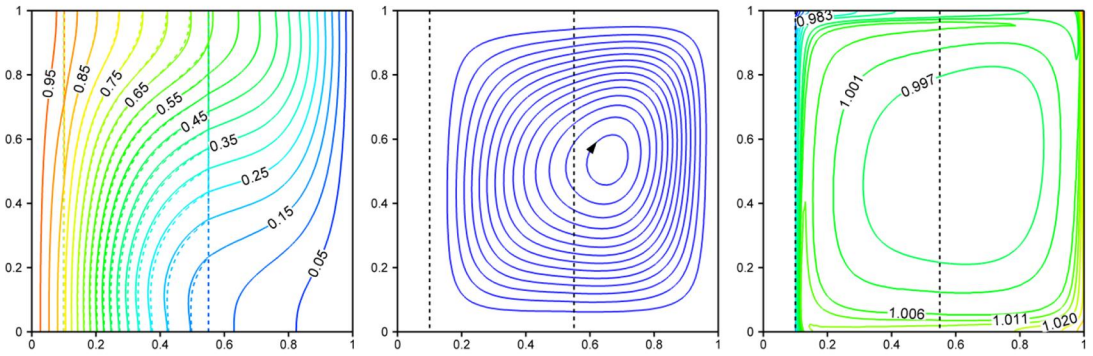

$\overline{Q_w} = 1.348,\ \overline{Nu_{nfp}} = 1.931,\ \overline{Nu_s} = 1.898,\ \overline{Nu_{nff}} = 1.348,\ |\Psi|_{max} = 2.901,\ \phi_{max} = 1.044$

(*c*)

Figure 7. Isotherms (left) (solid line for θ_{nf}, dashed line for θ_s), streamlines (middle), and isoconcentrations (right) for $Pr = 5$, $Nr = 10$, $Nb = 10^{-6}$, $Nt = 10^{-6}$, $Le = 10^3$, $D = 0.1$, $S = 0.45$, $K_r = 10$, $R_k = 1$, $\varepsilon = 0.6$: a) $Ra = 10^4$, $Da = 10^{-2}$, $H = 1$, b) $Ra = 10^5$, $Da = 10^{-3}$, $H = 1$, c) $Ra = 10^4$, $Da = 10^{-2}$, $H = 100$.

porous matrix average Nusselt number. Moreover, the value of the average heat transfer through the wall remains approximately constant by increasing the interface heat transfer coefficient. Variation of the interface heat transfer coefficient does not have significant effect on the flow pattern and the strength of the circulation cell inside the enclosure. It can be predicted from Figure 7*c* that at higher values of the interface heat transfer coefficient, the shapes of the isotherms of two different phases of

the porous medium become similar and the values of the average Nusselt number of the two phases become equal due to the large thermal interaction between the nanofluid and solid phases of the porous medium. Therefore, the thermal equilibrium condition is satisfied at higher values of the interface heat transfer coefficient.

Figure 8 presents the isotherms and streamlines to show the effect of buoyancy ratio parameter (Nr) on the thermal and flow filed inside the enclosure. The buoyancy ratio denotes the ratio of buoyancy force due to the mass transfer of nanoparticles to the buoyancy force due to heat transfer. The buoyancy force of mass transfer phenomenon is caused by the concentration difference of nanoparticles. In fact, the thermophoresis force tends to move the nanoparticles from the hot (vertical wall–porous interface) to the cold regions (the vertical boundary). Thus, this migration creates two different regions with high (heavy region) and low (light region) volume fractions of nanoparticles. The increase in buoyancy ratio parameter, Nr, raises the influence of the induced buoyancy force due to the concentration gradient of nanoparticles. As the nanofluid moves more freely in the free layer, the effect of buoyancy force due to the concentration gradient becomes more significant in the free layer, hence the center of the circulating cell shifts toward the free layer when $Nr = 20$.

Figures 9 and 10 show the effect of Rayleigh number (Ra) on the average Nusselt number of the nanofluid ($\overline{Nu_{nfp}}$) and solid porous matrix ($\overline{Nu_s}$) for different values of the Brownian motion (Nb) and thermophoresis (Nt) parameters. The results show that both of the average Nusselt numbers ($\overline{Nu_{nfp}}$ and $\overline{Nu_s}$) are an increasing function of Rayleigh number. As the Rayleigh number increases, the buoyancy force becomes stronger and the convection heat transfer dominates the heat transfer through conduction, which results in higher Nusselt numbers. Figure 9 shows that the increase in Nb leads to a slight increase in the average Nusselt number of the nanofluid, while the value of average Nusselt number for the solid matrix remains approximately constant at the considered range of Nb. In addition, contrary to the Brownian motion effect, increasing the thermophoresis parameter leads to a reduction in the magnitude of the nanofluid average Nusselt number (Figure 10). As mentioned earlier, the thermophoresis force is in direct relation to the temperature gradient from hot to cold. Therefore, as Nt increases, the diminution rate of nanoparticles concentration near the hot wall–porous interface intensifies, which cause a reduction of heat transfer rate. Furthermore, as is seen in Figure 10*b*, the variation of the average Nusselt number of the solid matrix with Nt is negligible. In general, the average Nusselt numbers change insignificantly with the variation of Brownian motion and thermophoresis parameters. A reason to justify such behavior could be that the coefficients of Nb and Nt in the dimensionless equations are very small. Hence, these parameters have little impact on the heat transfer rate.

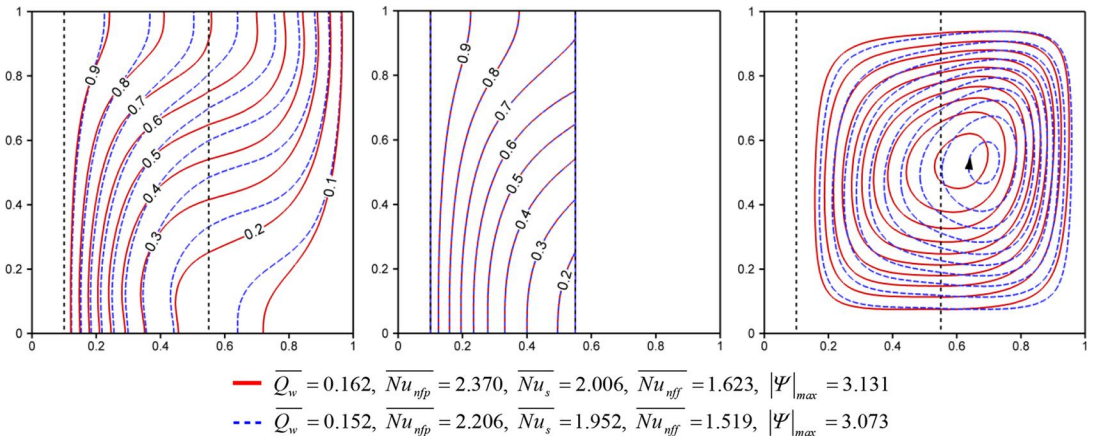

Figure 8. Isotherms for the nanofluid θ_{nf} (left), isotherms for the porous matrix θ_s (middle), and streamlines (right) for $Ra = 10^4$, $Da = 10^{-2}$, $Pr = 5$, $Nb = 10^{-6}$, $Nt = 10^{-6}$, $Le = 10^3$, $D = 0.1$, $S = 0.45$, $H = 10$, $K_r = 10$, $R_k = 10$, $\varepsilon = 0.6$, $Nr = 0$ (solid red line), and $Nr = 20$ (dashed blue line).

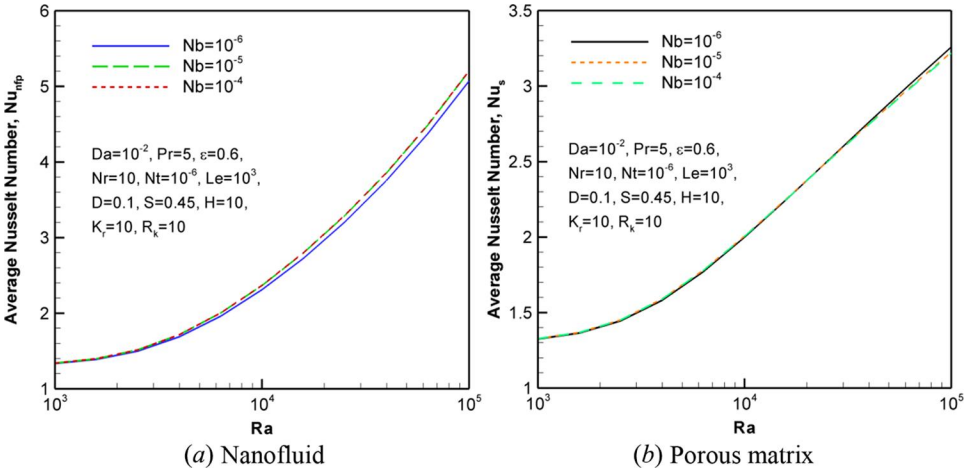

Figure 9. Variation of average Nusselt number for the nanofluid and the porous matrix with Ra number for different values of the Brownian motion parameter Nb.

Figure 11 illustrates the effects of Darcy number (Da) and porous layer thickness (S) on the average Nusselt numbers in the nanofluid and solid matrix of the porous layer. It can be observed that the enhancement of heat transfer rate starts at $\mathrm{Da} = 10^{-4}$, increases with a gentle slope until $\mathrm{Da} = 10^{-3}$, and then this rising trend continues with a steep slope until $\mathrm{Da} = 10^{-2}$ and after this value, the effect of Darcy number on increasing the heat transfer rate gradually diminishes. It should be noted that the Darcy number represents the permeability of the porous medium. As the Darcy number increases, more fluid flows through the porous region, hence the convection heat transfer becomes stronger. It can be concluded that rising trend of average Nusselt number as a function of Darcy number is due to the increase in the permeability of the porous medium and enhancement of the convection heat transfer in the porous layer. Increase in the average Nusselt number of the nanofluid phase has higher rate than the solid phase, and the difference between them becomes more significant at higher values of the Darcy number. In addition, Figure 11 illustrates that by increasing the porous layer thickness, the magnitude of the average Nusselt number of the both phases of the porous layer

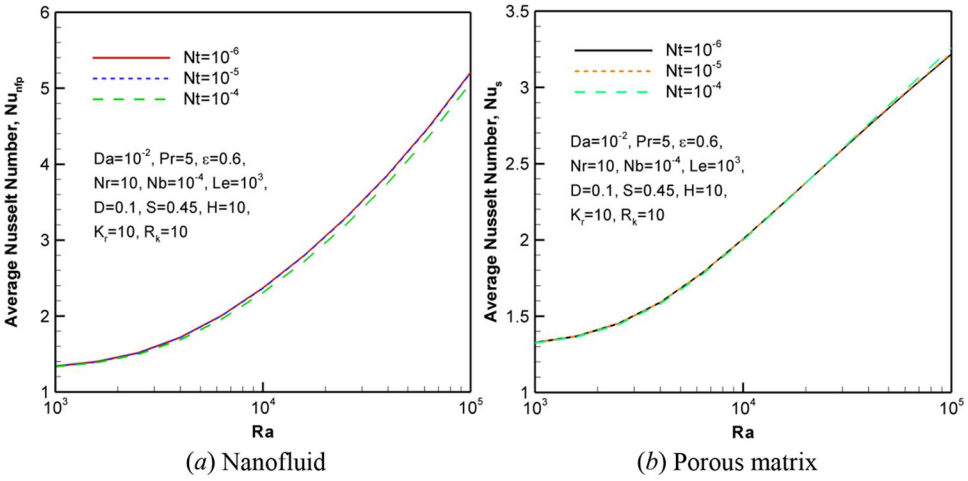

Figure 10. Variation of average Nusselt number for the nanofluid and the porous matrix with Ra number for different values of the thermophoresis parameter Nt.

decreases. This is because of the hydrodynamic resistance imposed by the porous layer, which is reinforced by increasing the porous layer thickness.

Similarly, to investigate the effect of porosity (ε) on the heat transfer rate, the variations of the average Nusselt numbers versus Darcy number are presented in Figure 12 at different porosities. Again, the results indicate that the average Nusselt numbers are increasing functions of the Darcy number at any considered value of the porosity. Moreover, as is seen in Figure 12, the average Nusselt numbers of both the nanofluid and solid matrix decrease with the increment in the porous medium porosity. In addition, the figure depicts that the heat transfer rate by nanofluid within the porous layer becomes smaller as the porosity increases. Furthermore, the average Nusselt number of the solid matrix decreases due to the direct interaction with the nanofluid.

It is worth pointing out that the effect of Prandtl number (Pr) within the wide range $5 \leq \mathrm{Pr} \leq 1000$ on the average Nusselt number for the nanofluid and solid porous matrix was studied. The variation of average Nusselt numbers with Pr showed almost a single curve for each phase of the porous medium, which indicates an insignificant effect of the Prandtl number on the heat transfer. Therefore, the effect of Prandtl number on the heat transfer has not been presented here for brevity.

Figure 13 depicts the effect of wall to nanofluid thermal conductivity ratio (R_k) on the average Nusselt numbers of the nanofluid and solid porous matrix for different values of the wall thickness. The results reveal that the average Nusselt numbers increase with the increase in wall to nanofluid thermal conductivity ratio parameter. Increasing R_k indicates the enhancement of wall conductivity, which causes more heat to reach the porous layer through the solid wall. The temperature difference between the two vertical faces of the porous layer increases, and consequently, the average Nusselt number for the nanofluid and solid matrix enhances. In addition, increasing the wall thickness leads to lower values of Nusselt numbers. The influence of wall thickness on the average Nusselt numbers is gradually weakened as R_k increases such that at high values of R_k (i.e., $R_k = 10$; highly conductive walls), the wall thickness does not have any significant effect on the average Nusselt numbers. This is due to the fact that at high conductivity ratio, the gained thermal energy by conduction through the wall overcomes the thermal resistance effect of the wall thickness. It is worth mentioning that for larger thickness of the wall, Nusselt number is more sensitive to the R_k values, as shown in Figure 13. In other words, at lower values of the wall thickness (i.e., $D = 0.01$), the wall to nanofluid thermal conductivity ratio has negligible effect on the magnitude of average Nusselt numbers particularly when $R_k \geq 1$.

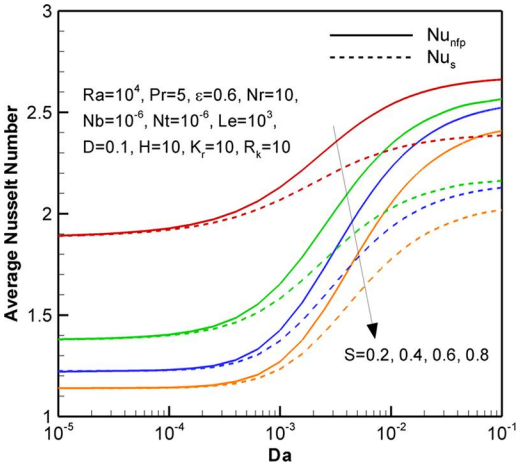

Figure 11. Variation of average Nusselt number for the nanofluid and the porous matrix with Da number for different values of the porous layer thickness *S*.

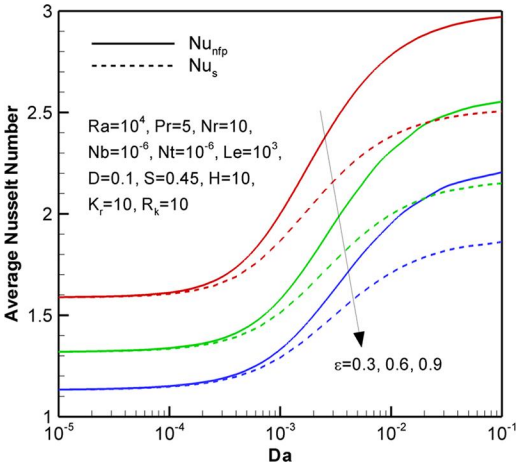

Figure 12. Variation of average Nusselt number for the nanofluid and the porous matrix with Da number for different values of porosity ε.

Figure 14 shows the effect of thermal conductivity ratio of the porous medium (K_r) on the average Nusselt number of the nanofluid and solid phases of the porous matrix. The increase in thermal conductivity ratio of the porous medium increases the average Nusselt number in both phases of the porous layer. This behavior corresponds to the fact that the increase in K_r indicates the thermal conductivity enhancement of the nanofluid compared to that of the solid porous matrix. Therefore, it is clear that in such a case, more heat is transferred through the nanofluid natural convection, as shown in Figure 14*a*. On the other hand, studying Eqs. (24) and (25) reveals that the variation of K_r can reduce or enhance the effect of interface heat transfer coefficient (H) in the heat transfer of the solid matrix phase. Hence, as the magnitude of K_r increases, the effect of thermal interaction between the nanofluid and solid matrix (i.e., H) intensifies. Note that the average Nusselt number in the solid matrix phase is an increasing function of H (Figures 7*a* and *c* and 15*b*). Therefore, the increase in K_r enhances the average Nusselt number in the solid porous matrix, as shown in Figure 14*b*.

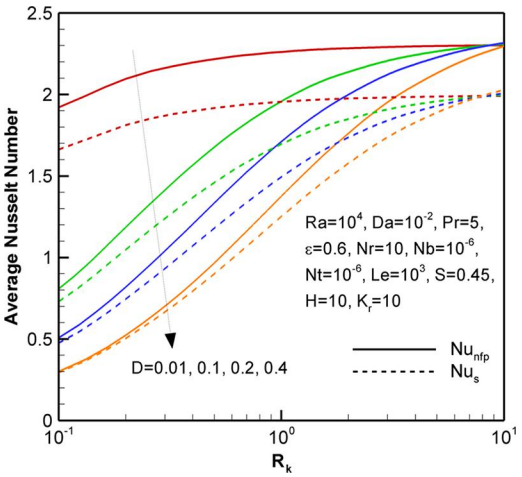

Figure 13. Variation of average Nusselt number for the nanofluid and the porous matrix with R_k for different values of the wall thickness D.

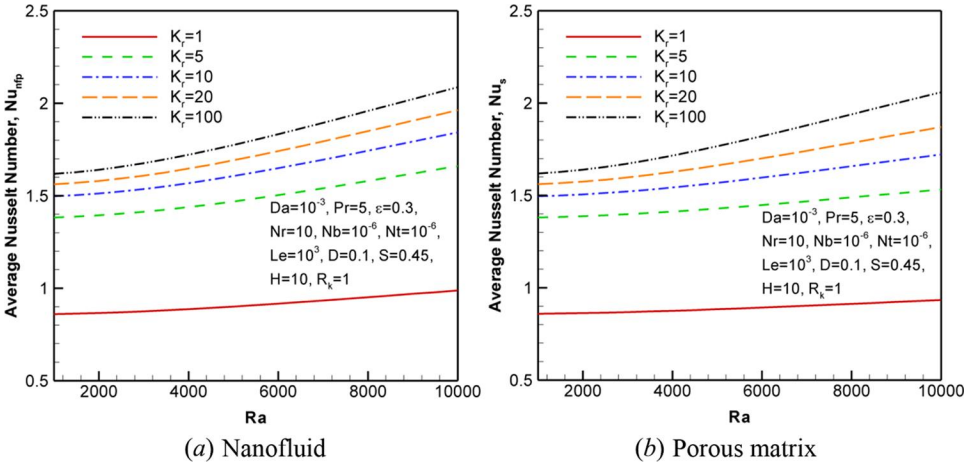

Figure 14. Variation of average Nusselt number for the nanofluid and the porous matrix with Ra number for different values of K_r.

Figure 15 shows the variation of average Nusselt numbers for the nanofluid and solid matrix as a function of buoyancy ratio parameter (Nr) at different values of H. It is observed that the increment of interface heat transfer coefficient reduces the average Nusselt number of the nanofluid. As previously mentioned, this is because of the thermal interaction augmentation between the nanofluid and solid porous matrix, which leads to a rise in the temperature of nanofluid. The rise of the nanofluid temperature near the hot wall reduces the temperature gradient and consequently reduces the average Nusselt number of the nanofluid. Due to transfer of the thermal energy from solid matrix to the nanofluid, the temperature of the solid porous matrix drops, hence the temperature difference between the solid matrix and hot wall increases. As a result, the average Nusselt number of the solid porous matrix increases, as is seen in Figure 15*b*. In addition, it can be deduced from the figures that the increase in buoyancy ratio parameter deteriorates the heat transfer rate through the porous layer. The reduction in average Nusselt number of the nanofluid (Figure 15*a*) is more significant in comparison to the solid porous matrix (Figure 15*b*). The increase in buoyancy ratio parameter intensifies the buoyancy force influence due to the mass transfer of nanoparticles. These effects are more pronounced near the vertical boundary where a thin boundary layer of nanoparticles is formed.

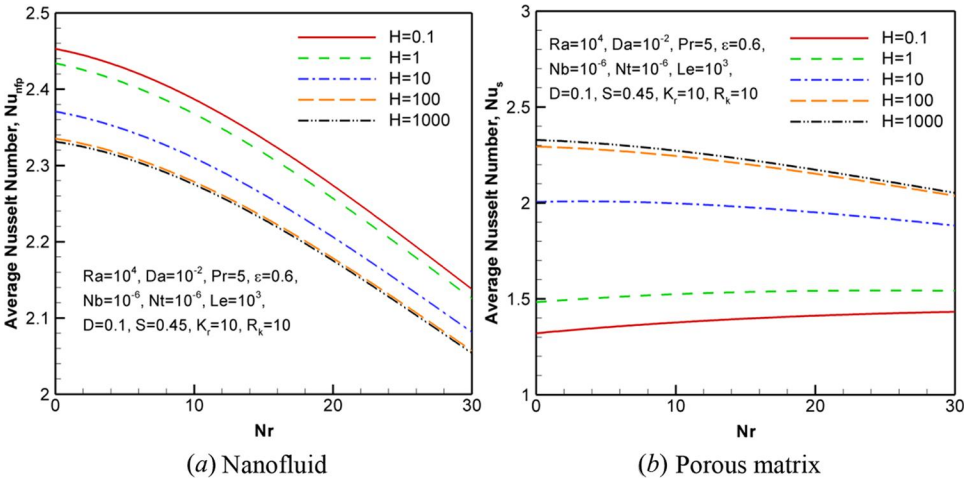

Figure 15. Variation of average Nusselt number for the nanofluid and the porous matrix with Nr for different values of H.

Therefore, the increase in buoyancy ratio parameter raises the vertical velocity of the nanofluid next to the vertical boundary, leading to a decrease in the average Nusselt number due to the temperature gradient reduction. These temperature variations of the nanofluid due to the indirect effect of the buoyancy ratio parameter variations affect the temperature gradient of the solid porous matrix. Hence, the average Nusselt number for the solid porous matrix smoothly drops by increasing the buoyancy ratio parameter, as shown in Figure 15*b*. However, it is worth mentioning that at lower values of H (i.e., $H = 1, 0.1$), the average Nusselt number for the solid matrix has an upward trend with increasing the buoyancy ratio parameter. This is because of the smaller thermal interaction between the two phases of porous medium at lower values of H, and consequently the reduction of indirect effect of the nanofluid due to the buoyancy force on the solid porous matrix.

7. Conclusion

The natural convective flow, heat and mass transfer of nanofluids in a cavity consisting of multilayers is studied using the Buongiorno's model and considering LTNE effects. In the cavity, there was a layer of solid wall over the hot wall, then a layer of porous medium was extended over the solid wall, and finally there was a layer of free fluid between the porous layer and the cold wall. The cavity was filled with nanofluid where drift flux of nanoparticles was allowed due to the thermophoresis and Brownian motion effects. The porous layer was modeled using the Darcy–Brinkman porous medium. A two-temperature model was used to take into account the temperature differences between the nanofluid and solid matrix phases using the LTNE model. Appropriate interface boundary conditions for the continuity of the temperatures and balance of energy at the porous layer interfaces are used. The nondimensional parameters are introduced to scale the model into a nondimensional form. The finite element method associated with a nonuniform grid structure was utilized to solve the governing differential equations. The results are reported for different parameters. The main findings of the present study can be summarized as follows:

1. Due to the thermophoresis effect, the nanoparticle concentration near the hot vertical interface of the wall–porous is low, while it is high near the cold vertical boundary.
2. When the convection interface heat transfer parameter (H) in the porous medium is low, i.e., $H \approx 10$, there is a significant difference between the temperature patterns of the nanofluid and the porous matrix in the porous layer. For the studied set of nondimensional parameters, the average Nusselt number of the nanofluid phase, $\overline{\mathrm{Nu}_{nfp}}$, in the porous medium layer is a decreasing function of H. In contrast, the average Nusselt number in the porous matrix phase, $\overline{\mathrm{Nu}_{s}}$, is an increasing function of H.
3. The increase in thickness of the porous layer (S) decreases the average Nusselt number for both phases of the nanofluid ($\overline{\mathrm{Nu}_{nfp}}$) and porous matrix ($\overline{\mathrm{Nu}_{s}}$) in the porous layer. However, the increase in wall thickness (D) decreases both of the Nusselt numbers of the porous layer, i.e., $\overline{\mathrm{Nu}_{nfp}}$ and $\overline{\mathrm{Nu}_{s}}$. The variation of the thermophoresis (Nt) and Brownian motion (Nb) parameters indicates a very slight effect on the average heat transfer.
4. The average Nusselt number in both phases of the porous medium, i.e., $\overline{\mathrm{Nu}_{nfp}}$ and $\overline{\mathrm{Nu}_{s}}$, is in increasing function of Ra and Da in all of the studied cases. The raise of the thermal conductivity ratios, i.e., K_r and R_k, also boosts both of the average Nusselt numbers in the porous layer.

ORCID

Mohammad Ghalambaz http://orcid.org/0000-0003-0965-2358

References

[1] P. Nithiarasu, K. N. Seetharamu, and T. Sundararajan, "Natural convective heat transfer in a fluid saturated variable porosity medium," *Int. J. Heat Mass Transfer*, vol. 40, pp. 3955–3967, 1997.

[2] B. Goyeau and D. Gobin, "Heat transfer by thermosolutal natural convection in a vertical composite fluid-porous cavity," *Int. Commun. Heat Mass Transfer*, vol. 26, pp. 1115–1126, 1999.
[3] C. Beckermann, S. Ramadhyani, and R. Viskanta, "Natural convection flow and heat transfer between a fluid layer and a porous layer inside a rectangular Enclosure," *J. Heat Transfer*, vol. 109, pp. 363–370, 1987.
[4] F. Wu, G. Wang, and W. Zhou, "A thermal nonequilibrium approach to natural convection in a square enclosure due to the partially cooled sidewalls of the enclosure," *Numer. Heat Transfer, Part A: Appl.*, vol. 67, pp. 771–790, 2015.
[5] K. Khanafer, K. Vafai, and M. Lightstone, "Buoyancy-driven heat transfer enhancement in a two-dimensional enclosure utilizing nanofluids," *Int. J. Heat Mass Transfer*, vol. 46, pp. 3639–3653, 2003.
[6] G. C. Bourantas, E. D. Skouras, V. C. Loukopoulos, and V. N. Burganos, "Heat transfer and natural convection of nanofluids in porous media," *Eur. J. Mech. - B/Fluids*, vol. 43, pp. 45–56, 2014.
[7] A. J. Chamkha and M. A. Ismael, "Conjugate heat transfer in a porous cavity filled with nanofluids and heated by a triangular thick wall," *Int. J. Therm. Sci.*, vol. 67, pp. 135–151, 2013.
[8] A. Brusly Solomon, M. Sharifpur, T. Ottermann, C. Grobler, M. Joubert, and J. P. Meyer, "Natural convection enhancement in a porous cavity with Al_2O_3-Ethylene glycol/water nanofluids," *Int. J. Heat Mass Transfer, Part B*, vol. 108, pp. 1324–1334, 2017.
[9] M. A. Sheremet, I. Pop, and R. Nazar, "Natural convection in a square cavity filled with a porous medium saturated with a nanofluid using the thermal nonequilibrium model with a Tiwari and Das nanofluid model," *Int. J. Mech. Sci.*, vol. 100, pp. 312–321, 2015.
[10] A. M. Rashad, M. M. Rashidi, G. Lorenzini, S. E. Ahmed, and A. M. Aly, "Magnetic field and internal heat generation effects on the free convection in a rectangular cavity filled with a porous medium saturated with Cu–water nanofluid," *Int. J. Heat Mass Transfer*, vol. 104, pp. 878–889, 2017.
[11] A. J. Chamkha and M. A. Ismael, "Natural Convection in Differentially Heated Partially Porous Layered Cavities Filled with a Nanofluid," *Numer. Heat Transfer, Part A: Appl.*, vol. 65, pp. 1089–1113, 2014.
[12] A. M. J. Al-Zamily, "Analysis of natural convection and entropy generation in a cavity filled with multi-layers of porous medium and nanofluid with a heat generation," *Int. J. of Heat Mass Transfer*, vol. 106, pp. 1218–1231, 2017.
[13] D. A. Nield, and A. Bejan, *Convection in Porous Media*, 4th ed., Springer, New York, 2013.
[14] K. Vafai and A. Amiri, "Non-Darcian effects in confined forced convective flows," *Trans. Phenom. Porous Media*, pp. 313–329, 1998.
[15] D. Das, P. Biswal, M. Roy, and T. Basak, "Role of the importance of 'Forchheimer term' for visualization of natural convection in porous enclosures of various shapes," *Int. J. Heat Mass Transfer*, vol. 97, pp. 1044–1068, 2016.
[16] J. C. Umavathi, O. Ojjela, and K. Vajravelu, "Numerical analysis of natural convective flow and heat transfer of nanofluids in a vertical rectangular duct using Darcy-Forchheimer-Brinkman model," *Int. J. Therm. Sci.*, vol. 111, pp. 511–524, 2017.
[17] A. K. Singh, P. Agnihotri, N. P. Singh, and A. K. Singh, "Transient and non-Darcian effects on natural convection flow in a vertical channel partially filled with porous medium: Analysis with Forchheimer–Brinkman extended Darcy model," *Int. J. Heat Mass Transfer*, vol. 54, pp. 1111–1120, 2011.
[18] M. Torabi, N. Karimi, K. Zhang, and G. P. Peterson, "Generation of entropy and forced convection of heat in a conduit partially filled with porous media – Local thermal non-equilibrium and exothermicity effects," *Appl. Therm. Eng.*, vol. 106, pp. 518–536, 2016.
[19] C. Sivaraj and M. A. Sheremet, "MHD natural convection in an inclined square porous cavity with a heat conducting solid block," *J. Magn. Magn. Mater.*, vol. 426, pp. 351–360, 2017.
[20] S. Mojumder, S. Saha, M. Rizwanur Rahman, M. M. Rahman, K. M. Rabbi, and T. A. Ibrahim, "Numerical study on mixed convection heat transfer in a porous L-shaped cavity," *Eng. Sci. Tech.*, vol. 20, pp. 272–282, 2017.
[21] V. Prasad and F. A. Kulacki, "Convective Heat Transfer in a Rectangular Porous Cavity—Effect of Aspect Ratio on Flow Structure and Heat Transfer," *J. Heat Transfer*, vol. 106, pp. 158–165, 1984.
[22] A. Baytas and I. Pop, "Free convection in a square porous cavity using a thermal nonequilibrium model," *Int. J. Therm. Sci.*, vol. 41, pp. 861–870, 2002.
[23] O. M. Haddad, M. A. Al-Nimr, and A. N. Al-Khateeb, "Validation of the local thermal equilibrium assumption in natural convection from a vertical plate embedded in porous medium: Non-Darcian model," *Int. J. Heat Mass Transfer*, vol. 47, pp. 2037–2042, 2004.
[24] A. I. Alsabery, A. J. Chamkha, H. Saleh, I. Hashim, and B. Chanane, "Effects of finite wall thickness and sinusoidal heating on convection in nanofluid-saturated local thermal non-equilibrium porous cavity," *Physica A: Statistical Mechanics and its Applications*, vol. 470, pp. 20–38, 2017.
[25] J. Buongiorno, "Convective Transport in Nanofluids," *J. Heat Transfer*, vol. 128, pp. 240–250, 2005.
[26] K. Ghasemi and M. Siavashi, "Lattice Boltzmann numerical simulation and entropy generation analysis of natural convection of nanofluid in a porous cavity with different linear temperature distributions on side walls," *J. Mol. Liq.*, vol. 233, pp. 415–430, 2017.
[27] M. A. Sheremet and I. Pop, "Conjugate natural convection in a square porous cavity filled by a nanofluid using Buongiorno's mathematical model," *Int. J. Heat Mass Transfer*, vol. 79, pp. 137–145, 2014.

[28] G. Kefayati and N. A. Che Sidik, "Simulation of natural convection and entropy generation of non-Newtonian nanofluid in an inclined cavity using BuongiornO's mathematical model (Part II, entropy generation)," *Powder Technol.*, vol. 305, pp. 679–703, 2017.
[29] S. Yekani Motlagh, S. Taghizadeh, and H. Soltanipour, "Natural convection heat transfer in an inclined square enclosure filled with a porous medium saturated by nanofluid using Buongiorno's mathematical model," *Adv. Powder Technol.*, vol. 27, pp. 2526–2540, 2016.
[30] S. Y. Motlagh and H. Soltanipour, "Natural convection of Al_2O_3-water nanofluid in an inclined cavity using BuongiornO's two-phase model," *Int. J. Therm. Sci.*, vol. 111, pp. 310–320, 2017.
[31] D. A. Nield and A. V. Kuznetsov, "The Cheng–Minkowycz problem for natural convective boundary-layer flow in a porous medium saturated by a nanofluid," *Int. J. Heat Mass Transfer*, vol. 52, pp. 5792–5795, 2009.
[32] H. Zargartalebi, A. Noghrehabadi, M. Ghalambaz, and I. Pop, "Natural convection boundary layer flow over a horizontal plate embedded in a porous medium saturated with a nanofluid: Case of variable thermophysical properties," *Trans. Porous Media*, vol. 107, pp. 153–170, 2015.
[33] K. Vafai and S. J. Kim, "On the limitations of the Brinkman-Forchheimer-extended Darcy equation," *Int. J. Heat Fluid Flow*, vol. 16, pp. 11–15, 1995.
[34] K. Vafai and C. L. Tien, "Boundary and inertia effects on flow and heat transfer in porous media," *Int. J. Heat Mass Transfer*, vol. 24, pp. 195–203, 1981.
[35] D. Y. Tzou, "Thermal instability of nanofluids in natural convection," *Int. J. Heat Mass Transfer*, vol. 51, pp. 2967–2979, 2008.
[36] H. Zargartalebi, M. Ghalambaz, A. Noghrehabadi, and A. J. Chamkha, "Natural convection of a nanofluid in an enclosure with an inclined local thermal non-equilibrium porous fin considering Buongiorno's model," *Numer. Heat Transfer, Part A: Applications, vol* 70, pp. 432–445, 2016.
[37] B. Alazmi and K. Vafai, "Analysis of fluid flow and heat transfer interfacial conditions between a porous medium and a fluid layer," *Int. J. Heat Mass Transfer*, vol. 44, pp. 1735–1749, 2001.
[38] K. Vafai and R. Thiyagaraja, "Analysis of flow and heat transfer at the interface region of a porous medium," *Int. J. Heat Mass Transfer*, vol. 30, pp. 1391–1405, 1987.
[39] J. Ochoa-Tapia and S. Whitaker, "Momentum transfer at the boundary between a porous medium and a homogeneous fluid—I. Theoretical development," *Int. J. Heat Mass Transfer*, vol. 38, pp. 2635–2646, 1995.
[40] L. Betchen, A. G. Straatman, and B. E. Thompson, "A nonequilibrium finite-volume model for conjugate fluid/porous/solid domains," *Numer. Heat Transfer, Part A: Applications*, vol. 49, pp. 543–565, 2006.
[41] K. Yang and K. Vafai, "Restrictions on the validity of the thermal conditions at the porous-fluid interface—an exact solution," *J. Heat Transfer*, vol. 133, pp. 112601–112601-12, 2011.
[42] N. Saeid, "Conjugate natural convection in a porous enclosure sandwiched by finite walls under thermal nonequilibrium conditions," *J. Porous Media*, vol. 11, pp. 259–275, 2008.
[43] D. Das, P. Biswal, M. Roy, and T. Basak, "Role of the importance of 'Forchheimer term' for visualization of natural convection in porous enclosures of various shapes," *Int. J. Heat Mass Transfer*, vol. 97, pp. 1044–1068, 2016.
[44] V. Prasad and F. A. Kulacki, "Convective heat transfer in a rectangular porous cavity—effect of aspect ratio on flow structure and heat transfer," *J. Heat Transfer*, vol. 106, pp. 158–165, 1984.
[45] J. N. Reddy, *An Introduction to the Finite Element Method*. McGraw-Hill: New York, 1993.
[46] S. S. Rao, *The Finite Element Method in Engineering*. Oxford, UK: Butterworth-Heinemann, 2005.
[47] P. Wriggers, *Nonlinear Finite Element Methods*. Berlin, Germany: Springer Science & Business Media, 2008.
[48] T. Basak, S. Roy, and A. R. Balakrishnan, "Effects of thermal boundary conditions on natural convection flows within a square cavity," *Int. J. Heat Mass Transfer*, vol. 49, pp. 4525–4535, 2006.
[49] T. Basak, S. Roy, A. Singh, and A. R. Balakrishnan, "Natural convection flows in porous trapezoidal enclosures with various inclination angles," *Int. J. Heat Mass Transfer*, vol. 52, pp. 4612–4623, 2009.
[50] M. Celli, "Non-homogeneous model for a side heated square cavity filled with a nanofluid," *Int. J. Heat Fluid Flow*, vol. 44, pp. 327–335, 2013.